

Molecular dynamics simulations of the evaporation of particle-laden droplets

Weikang Chen^{1,3,*}, Joel Koplik^{1,3,†} and Ilona Kretzschmar^{2‡}
Benjamin Levich Institute¹ and Departments of Chemical Engineering² and Physics³
City College of the City University of New York, New York, NY 10031
(Dated: November 11, 2018)

We use molecular dynamics simulations to study the evaporation of particle-laden droplets on a heated surface. The droplets are composed of a Lennard-Jones fluid containing rigid particles which are spherical sections of an atomic lattice, and heating is controlled through the temperature of an atomistic substrate. We observe that sufficiently large (but still nano-sized) particle-laden drops exhibit contact line pinning, measure the outward fluid flow field which advects particle to the drop rim, and find that the structure of the resulting aggregate varies with inter-particle interactions. In addition, the profile of the evaporative fluid flux is measured with and without particles present, and is also found to be in qualitative agreement with earlier theory. The compatibility of simple nanoscale calculations and micron-scale experiments indicates that molecular simulation may be used to predict aggregate structure in evaporative growth processes.

The evaporation of a sessile droplet on a hot surface is a key problem in fluid mechanics, relevant both to theoretical issues in heat transfer and to practical questions in materials processing. The evaporation of a *particle-laden* droplet raises the additional issue of the structure of the resulting solid aggregate, and, going further, offers the possibility of controlling this structure by means of anisotropic (*e.g.*, Janus) surface properties [1]. A familiar and paradigmatic example of this process occurs in coffee stains, where the residue of evaporated droplets takes the form of a ring-like deposit of grains at the rim. Experiments by Deegan and collaborators [2] focused attention on this “coffee ring problem” several years ago, and subsequent work [3–6] established the ubiquity of the process, while numerous theoretical studies have addressed the dynamics [7–11]. A complete understanding of the problem is not yet available however: experiments cannot measure everything in a small, time-dependent, multiphase droplet, while most theoretical treatments require approximations to deal with an evaporating particle-laden drop.

In this paper we use molecular dynamics (MD) simulations to simulate the evaporation of droplets containing colloidal particles, having either uniform or Janus-like surface properties. One goal is to test whether the phenomena found in micron-sized particle systems persist down to nanometer scales; in this way we hope to extend the size range in which controlled aggregate structures may be produced by droplet evaporation. A second goal is to test the validity of some of the underpinnings of the theoretical analyses used in the problem. Since MD simulations provide detailed atomic-scale information, we can measure concentration, temperature and fluid flow, even during the rapid heterogeneous processes occurring in evaporation. The difficulties of applying uncertain constitutive relations are absent, although replaced to some degree by the problem of extracting a robust signal from a relatively small sample in a fluctuating environment. More generally, our goal is to establish the ability of these

relatively basic simulations of moderate scale systems to predict phenomena occurring in droplet evaporation and guide experimental investigations.

The simulations use standard molecular dynamics (MD) techniques [12–14] and generic interactions of Lennard-Jones form,

$$V(r_{ij}) = 4\epsilon \left[\left(\frac{\sigma}{r_{ij}} \right)^{12} - \left(\frac{\sigma}{r_{ij}} \right)^6 \right] \quad (1)$$

For simplicity we assume that all fluid and particle atoms have the same interaction potential, along with the same mass m and approximate diameter σ . The calculations are nondimensionalized using ϵ , σ and m as energy, length and mass scales, respectively, and the resulting time scale is $\tau = \sigma(m/\epsilon)^{1/2}$. Typical numerical values are $\sigma \sim 0.3\text{nm}$, $\tau \sim 2\text{ps}$ and $\epsilon \sim 120k_B$, where k_B is Boltzmann’s constant, and temperatures are measured in units of ϵ/k_B . The fluid atoms in liquid or vapor obey ordinary Newtonian dynamics with the force arising from the interaction with other atoms (within a cutoff radius of 2.5σ), using a predictor-corrector method for the integration of the equations of motion. The particles are spherical sections of an atomic fcc lattice containing all atoms within a certain radius of a center; here the atomic density is 0.8, the radius is 2 and the particles contain 32 atoms. These are Janus particles, implemented by making the atoms in only one hemisphere of a particle attractive to other particle atoms; all particle atoms attract the fluid and wall in the same way. The particles move as rigid bodies, where the net force and torque on each particle is computed by summing the interatomic forces between its atoms and the neighboring fluid atoms, and the motion is given by the Newton and Euler equations. Quaternion variables are used to describe the particle orientations [12]. The solid substrate is made of atoms coupled to fcc lattice sites by a linear spring of stiffness $100\epsilon/\sigma^2$.

Initially the drop consists of a hemispherical cap of 72,236 fluid atoms placed above a (monolayer) solid wall.

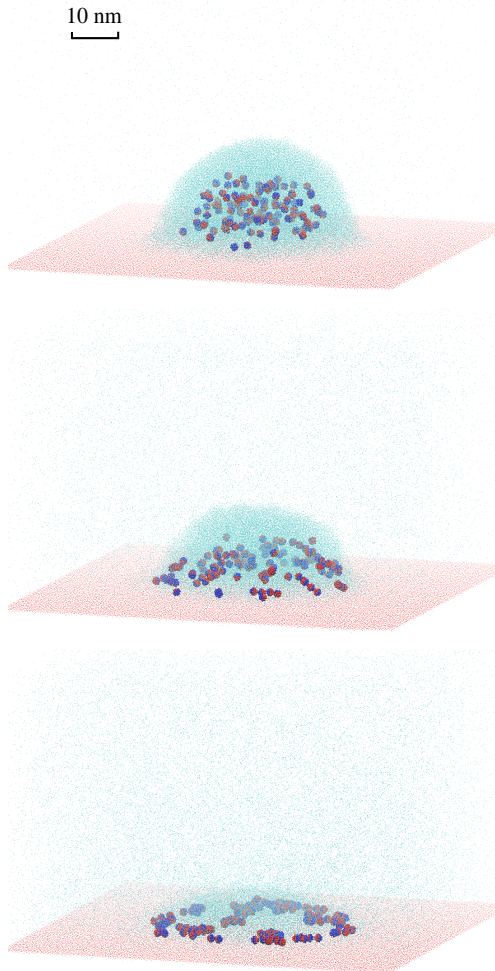


FIG. 1. (Color online) Evaporation of a particle-laden droplet: fluid and solid atoms are shown as cyan and red dots respectively and the Janus particles are circles whose two sides are red and blue. Top to bottom: times 50 , 500 and 1000τ .

119 particles of 32 atoms each are centered at random positions within the cap, and the entire system is equilibrated by gradually raising the temperature from 0.5 to 1.2 using velocity rescaling, following which the substrate is maintained at this temperature while the fluid temperature is allowed to vary. The liquid expands slightly during the temperature ramp and then, as seen in Fig. 1, the drop shrinks monotonically as it emits vapor, and eventually disappears due to evaporation. Evaporating fluid atoms which leave the simulation box are simply deleted. Meanwhile the particles settle towards the substrate and subsequently are advected to the rim of the droplet and deposit there. The contact line itself remains pinned. The connection between liquid and particle motion is indicated by the velocity field shown in Fig. 2: the fluid moves downward over most of the drop and radially outward near the substrate. This velocity field is com-

puted by dividing the simulation domain into concentric circular rings along the vertical axis of the drop, and simply averaging the atomic velocities in each ring.

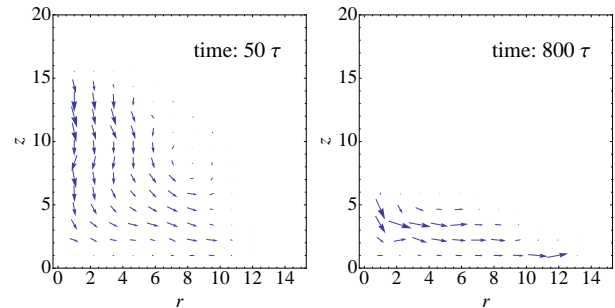


FIG. 2. Velocity field in cylindrical coordinates in an evaporating particle-laden droplet at early and late times; the solid occupies the region $z < 0$.

The origin of the flow that drives particles to the rim is, it is believed [2], contact line pinning coupled to the fact that the evaporative flux is largest at the edges of the drop. The liquid must supply this flux as the droplet shrinks down, and the geometry of the situation requires a strong outward flow field, as seen in Fig. 2. More precisely, for drops of pure liquid evaporating with a fixed contact line, one can show [9, 10, 15, 16] that

$$j(r, \theta) = j_0 \left(1 - \frac{r^2}{R^2}\right)^{-\lambda(\theta)} \quad \lambda(\theta) = \frac{1}{2} \left(1 - \frac{\theta}{\pi - \theta}\right) \quad (2)$$

Here, θ is the contact angle between the droplet and the wall, which varies as the droplet evaporates. The key point is that for $\theta < \pi/2$ the (mathematical) vapor flux diverges at the edge of the droplet. Of course, there is no real singularity in a physical problem, and one expects j to be cut off at a small (molecular) scale.

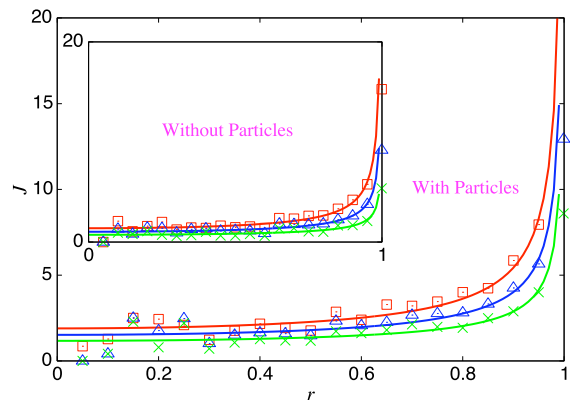


FIG. 3. (Color online) Evaporative vapor flux vs. scaled radius for particle laden-drops and, in the inset, for pure fluid drops. The three curves refer to times 300τ (\times , green), 400τ (Δ , blue) and 500τ (\square , orange).

We have measured the evaporative flux both for pure liquid and particle-laden drops, and obtained Fig. 3, which shows $j(r, t)$ at the three successive times indicated. Each plot is an average over a short (10τ) interval centered at 300, 400 and 500τ . Averaging is necessary to smooth the fluctuations, and longer averaging periods would be more effective, but the drop shape changes too much over longer intervals. The entire evaporation process lasts for about 1000τ (roughly 2 ns) for the Janus case, and slightly longer for pure fluid evaporation, but the data at later times involves fewer and fewer evaporating atoms and is too noisy for analysis. The ordinate in Fig. 3 is radial position divided by the current drop radius, and varies between 0 and 1. While the radius is constant (except for fluctuations) in the particle-laden case, the radius of the pure fluid drop decreases with time. We see that indeed the vapor current tends to diverge at the rim and the divergence increases with time. This behavior is qualitatively consistent with Eq. 2, since a stronger divergence requires a smaller contact angle, and the simulations show this trend. However, the formula fails to quantitatively describe the simulations. The exponents $\lambda(\theta)$ obtained in fitting the pure fluid data are 0.48, 0.55 and 0.60 at times 300, 400 and 500τ , respectively, but Eq. 2 does not permit values $\lambda > 1/2$. Some possible explanations for this discrepancy are deviations from bulk continuum behavior in nanosized regions, difficulties in measuring the flux accurately in directions nearly parallel to the surface, and inadequate ensemble averaging in obtaining the data. The flux is slightly more singular for the particle-laden drop: the fitted values of λ are 0.53, 0.58 and 0.62 for the same three times.

Not all evaporating nanodrops behave in this way. One important requirement for obtaining a deposit at the rim is that the drop be large enough: if the drop is too small it evaporates, or at least decays into a thin pancake, before the flow field is established and the particles are able to move to the rim. This behavior was first observed experimentally by Shen *et al.* [17], and we have reproduced it in simulations. The drop shown in Fig. 1 has a radius of about 20 nm, whereas in similar simulations for drops whose initial radius is 5 or 10 nm we see that the particles deposit roughly uniformly over the drops interior; see Fig. 4.

A second constraint needed for deposition to occur at the drop rim is that the liquid must have adequate thermal contact with the solid to set up the flow field seen above [18]. We have investigated this issue by varying the interaction between the liquid and the wall: in the Lennard Jones potential (Eq. 1) acting between fluid and wall atoms, we varied the coefficient of the attractive r^{-6} term between 0 (pure short-distance repulsion - hydrophobic wall) and 1 (standard strength attraction - completely wetting wall) and observed the resulting solid pattern while measuring the thermal conductivity. The latter simulation involved a slab of liquid completely fill-

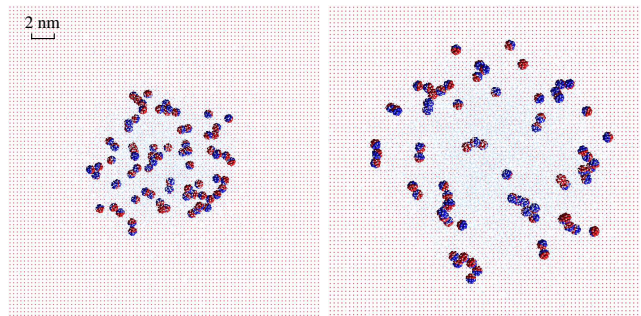


FIG. 4. (Color online) Particle deposit for evaporated drops of initial radius (left) 5 and (right) 10 nm. The color scheme is given in the caption to Fig. 1.

ing the gap between two atomic walls held at different temperatures. As the attractive strength decreased from 1 to 0 the thermal conductivity decreased approximately linearly, ultimately by a factor of nearly 10. Correspondingly, as the wall attractive strength decreased the resulting pattern of solid particles varied from the rim deposit shown above to a crystallized droplet. The effects of substrate thermal resistance and conductivity on evaporation have been studied more systematically by Dunn *et al.* [19, 20].

The detailed structure of the deposit is an important consideration in potential applications to evaporative self-assembly. We saw above that particles with Janus surface properties would, under the right conditions, form a rim deposit with chain-like structures. This behavior is confirmed by experimental observations of gold-capped sulfated-polystyrene Janus particle-laden droplets during drying [21]. The chaining behavior is a result of the attractive interaction between the gold caps of and the sulfated polystyrene half of the Janus particles.

Additional experiments investigated the effect of particle surface charge on the deposition behavior [21, 22]. The presence of sulfate groups on the surface of the particles results in an overall negative charge, which can be screened by the addition of salt. Sulfated polystyrene particles in distilled water form hexagonal close-packed, highly ordered layers at the rim, whereas formation of randomly packed particle layers is observed in 10 mM aqueous NaCl solution. These results motivated us to study the effect of charge on the deposit structure of uniform particles. In Fig. 5, we show the deposits that result when the charge on a symmetric particle increases from 0 to 4 and then to 8. In the simulations, a charge of the appropriate magnitude is placed at the center of the particle, and a Coulomb interaction is applied. The neutral case resembles the random packing observed in the 10 mM case. The charge 8 situation models the case where the particles carry a charge, *i.e.*, deposition in deionized water. It is apparent from the bottom panel of Fig. 5 that the particles tend toward assembling at the rim and a

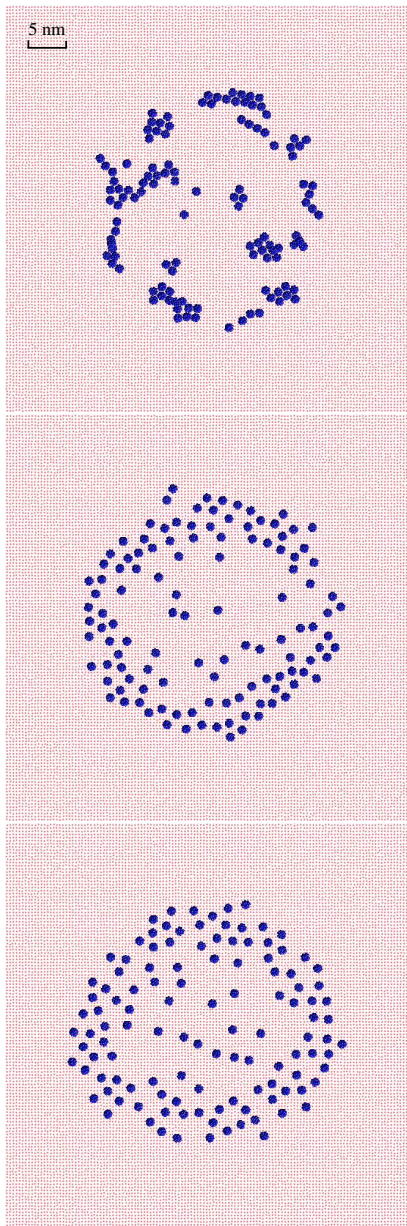


FIG. 5. Effects of adding a charge to a plain (non-Janus) particle. Top to bottom: charge 0, 4 and 8.

regular packing [23], but that the drop volume is not sufficient to enable long enough evaporation times to achieve close packing at the rim.

We have shown that straightforward, medium-scale MD simulations can easily capture most of the salient features in the evaporation of particle-laden droplets. Aside from demonstrating that nano-scale and micron-scale systems behave in a similar way with regard to the behavior of the particles, we were able to measure continuum fields such as velocity within the droplet, along with the profile of the evaporative flux, which drives the process. Using standard methods, we have also measured (but not reported here) the density, temperature, concen-

tration and stress fields within the droplet. In addition, we were able to show the existence of a minimum drop size for rim deposition, and verify the importance of adequate thermal coupling between liquid and solid. Furthermore, the simulations give the connection between particle interactions and deposit structure. The significance of these results is that simple simulations provide a viable method for both testing the theoretical underpinnings of the process and for predicting the nature of the outcome – the structure of the resulting particle deposit. In this paper we have focused on the most important aspect of the continuum flow, the velocity field and the evaporative flux, but any other quantity which can be determined from atomic variables is equally accessible.

This work was supported in part by NSF-CBET (CA-REER) 0644789.

* wchen@ccny.cuny.edu

† kopluk@sci.cuny.cuny.edu

‡ kretzschmar@ccny.cuny.edu

- [1] S. Jiang, Q. Chen, M. Tripathy, E. Luitjen, K. S. Schweitzer and S. Granick, *Adv. Mater.* **22**, 1060 (2010).
- [2] R. D. Deegan, O. Bakajin, T. F. Dupont, G. Huber, S. R. Nagel and T. A. Witten, *Nature* **389**, 827 (1997).
- [3] R. D. Deegan, *Phys. Rev. E* **61**, 475 (2000).
- [4] T. P. Bigioni, X.-M. Lin, T. T. Nguyen, E. I. Corwin, T. A. Witten and H. M. Jaeger, *Nature Mater.* **5**, 265 (2006).
- [5] H. Bodihuel and J. Lang, *Soft Matter* **6**, 5451 (2010).
- [6] R. Bhardwaj, X. Feng, P. Somasundaran and D. Astinger, *Langmuir*, **26**, 7833 (2010).
- [7] R. D. Deegan, O. Bakajin, T. F. Dupont, G. Huber, S. R. Nagel and T. A. Witten, *Phys. Rev. E* **62**, 756 (2000).
- [8] Y. O. Popov, *Phys. Rev.* **71**, 036313 (2005).
- [9] T. Okuzono, M. Kobayashi and M. Doi, *Phys. Rev. E* **80**, 021603 (2009).
- [10] A. Cazabat and G. Guéna, *Soft Matter* **6**, 2591 (2010).
- [11] K. L. Maki and S. Kumar, *Langmuir*, **27**, 11347 (2011).
- [12] M. P. Allen and D. J. Tildesley, *Computer Simulation of Liquids* (Oxford, New York, 1987)
- [13] D. Frenkel and B. Smit, *Understanding Molecular Simulation*, 2nd ed. (Academic, New York, 2002).
- [14] D. C. Rapaport. *The Art of Molecular Dynamics Simulation*, 2nd ed. (Cambridge, New York, 1995)
- [15] H. Hu and R.G. Larson, *J. Phys. Chem. B* **106**, 1334 (2002).
- [16] H. Hu and R.G. Larson, *Langmuir* **21**, 3963 (2005).
- [17] X. Shen, C.-M. Ho and T.-S. Wong, *J. Phys. Chem B* **114**, 5269 (2010)
- [18] B. H. Kim, A. Beskok and T. Cagiri, *J. Chem. Phys.* **129**, 174701 (2008).
- [19] G.J. Dunn, S. K. Wilson, B. R. Duffy, S. David and K. Sefiane, *J. Fluid Mech.* **623**, 329 (2009).
- [20] G.J. Dunn, S. K. Wilson, B. R. Duffy, and K. Sefiane, *Phys. Fluids* **21**, 052101 (2009).
- [21] F. Guzman, E. Cranston, M. Rutlend and I. Kretzschmar, to be published (2012).
- [22] S. C. Rödner, P. Wedin and L. Bergstrom, *Langmuir* **18**,

9327 (2002).

[23] Y. K. Koh and C.C. Wong, *Langmuir* **22**, 897 (2006).